Annals of Nuclear Medicine Vol. 8, No. 4, 277–281, 1994

Simulation study of triple-energy-window scatter correction in combined Tl-201, Tc-99m SPECT

Koichi OGAWA

Department of Electronic Informatics, College of Engineering, Hosei University

In a quantitative SPECT study with multiple radionuclides, it is very important to eliminate the counts of scattered photons from planar images. In this paper, the triple energy window (TEW) method, which has developed to eliminate the counts of scatter photons in measured counts, was applied to a multiradionuclide SPECT study and its effect was examined in a simulation study. In the simulation, we used Tc-99m and Tl-201, and we assumed their photopeak energies to be 141 and 73 keV, respectively. For two different activity distributions in a cylinder phantom, simulation tests with Tl-201 and Tc-99m gave good agreement between the activity distributions reconstructed from primary photons and those from corrected data. The contrast of a cold spot area in images with and without correction improved around 70% to more than 96%.

Key words: scatter correction, single photon emission CT, multiradionuclide study

INTRODUCTION

IN RADIONUCLIDE IMAGING with a gammacamera, the amount of scattered photons measured by means of a photopeak energy window is more than one-third of the total amount of the measured photons.[1] Moreover, the amount of the scattered photons varies pixel by pixel in a planar image depending on many factors, which include object sizes, source distributions, and source energies.[1–3] Therefore, in order to reconstruct a quantitative single photon emission CT (SPECT) image, it is important to remove the count of scattered photons from the measured count considering these factors. Many methods were proposed to eliminate the counts of scattered photons from planar images or reconstructed images; there were (1) the deconvolution method,[4] (2) the dual energy window subtraction method,[5,6] (3) the energy-weighted acquisition method,[7] (4) the iterative peak erosion algorithm and the spectral-fitting algorithm,[8] (5) the factor analysis method,[9] (6) the inverse Monte Carlo reconstruction algorithm,[10] (7) the asymmetrically high offset photopeak window method,[11] (8) the dual photopeak window method,[12] and (9) the triple energy window (TEW) method.[13] Using the above methods, we can reduce the counts of scattered photons in a single radioisotope SPECT study.

Recently, some SPECT studies have used two radioisotopes such as Tc-99m and Tl-201, or I-123 and Tl-201, simultaneously. For simplicity, we will hereafter use the term multiradionuclide study to mean a study using two radionuclides. In the multiradionuclide study, Compton photons due to high-energy primary photons enter the energy window of the low-energy photopeak, and therefore the count of the low-energy photopeak window increases. Moreover, the count is also affected from the Compton photons due to the low-energy primary photons. However, the conventional scatter correction methods have not usually been applied to multiradionuclide. On the other hand, our proposed method (TEW)[13,14] is applicable to the multiradionuclide SPECT study and the method is simpler and more practical than the above methods. The TEW method, however, requires strict uniformity in several narrow energy ranges around the photopeak energy. This condition is needed for most of the above-mentioned correction methods. In the TEW method, a main window centered at photopeak energy and two subwindows on both sides of the main window are set for each photopeak, and the counts of these windows are measured for each pixel in each planar image. Then the count of the scattered photons included in each main window is estimated from the counts for the subwindows and is subtracted from that of the main window. In this paper, by means of a Monte Carlo simulation, we quantitatively clarified the validity of the TEW method in the

Received June 23, 1994, revision accepted August 8, 1994.

For reprint contact: Koichi Ogawa, Ph.D., Department of Electronic Informatics, College of Engineering, Hosei University, 3–7–2 Kajinocho, Koganei, Tokyo 184, JAPAN.

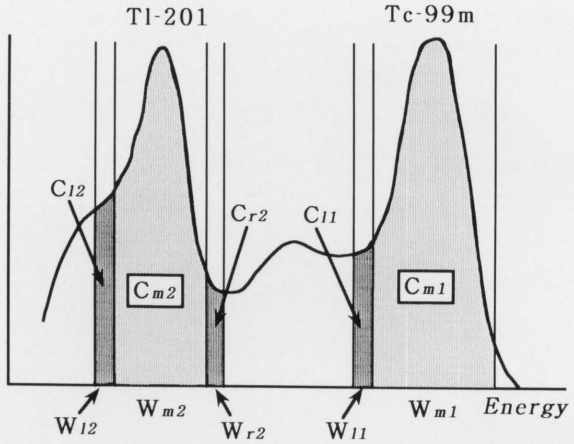

Fig. 1 Location and width of the windows. For each photopeak, a main window and two subwindows are positioned. C_l, C_m, and C_r indicate the count of the left, middle, and right window, respectively. W_l, W_m, and W_r mean the width of the left, middle, and right window, respectively.

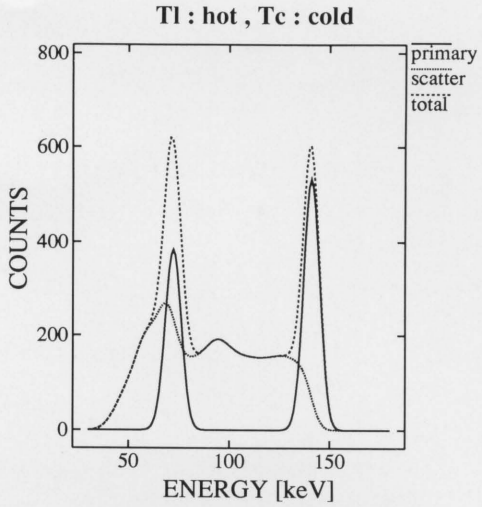

Fig. 2 Energy spectra of primary photons and scatter photons.

application of a multiradionuclide SPECT study.

METHODS

In the application of the TEW method to a multiradionuclide SPECT study with Tc-99m and Tl-201, the energy windows are set as shown in Figure 1. The count of primary photons for each photopeak is estimated with the main window centered at the photopeak energy and two subwindows on both sides of the main window. The count of the primary photons in each photopeak is given by

$$C_{p1} = C_{m1} - \left(\frac{C_{l1}}{W_{l1}}\right) \cdot \frac{W_{m1}}{2} \quad (1)$$

$$C_{p2} = C_{m2} - \left(\frac{C_{l2}}{W_{l2}} + \frac{C_{r2}}{W_{r2}}\right) \cdot \frac{W_{m2}}{2} \quad (2)$$

where C_{m1} and C_{m2} are the counts measured by the main window, and the count is composed of the count of primary photons C_{p1} and C_{p2} and those of scattered photons. W_{m1} and W_{m2} are the widths of the main window, and (W_{l1}, W_{r1}) and (W_{l2}, W_{r2}) are those of subwindows. From the counts acquired by the two subwindows C_{l1} and $C_{r1}(=0)$, and C_{l2} and C_{r2}, the scattered photons are estimated by a trapezoidal rule. With the equations we can estimate the count of primary photons at each pixel. In estimating the count of primary photons in the high-energy photopeak, we make C_{r1} zero to avoid the effects of statistical noise. Since the count for the right subwindow (C_{r1}) will be only a few percent of that of the main window, it may be insignificant in estimating scattered photons.

SIMULATIONS

For a model of the multiradionuclide SPECT study, Tc-99m and Tl-201 were used, and their photopeak energies were assumed to be 141 keV and 73ke V, respectively. We used the water-filled cylindrical phantom (radius: 10 cm), in which a small water-filled cylinder (radius: 3 cm) is located off center, and assumed the cylinders had infinite length. With the cylinder phantom, we could define two types of activity distributions, that is, the cold spot phantom and the hot spot phantom. In the cold spot phantom, named cold spot, the activity was only distributed in the large outer cylinder, and in the hot spot phantom, named hot spot, the activity was only distributed in the small inner cylinder. Moreover, by considering the two radionuclides (Tc-99m and Tl-201), we defined four cases of activity distributions, that is, (1) case 1: Tl cold spot with Tc cold spot, (2) case 2: Tl hot spot with Tc cold spot, (3) case 3: Tl cold spot with Tc hot spot, and (4) case 4: Tl hot spot with Tc hot spot. The activity ratio of Tl to Tc was 1 : 1. To calculate the energy spectrum at each pixel position in each projection, a Monte Carlo simulation[15] was carried out in the same manner as in previous papers.[1] The simulation was performed separately for Tl-201 and Tc-99m in each case, and count data for a specified window were obtained by integrating the energy spectrum. The trajectory numbers were 100,000,000 photons for the cold spot phantom and 10,000,000 photons for the hot spot phantom for Tc-99m and Tl-201. For the energy resolution (FWHM) of the scintillator, we used 15.5 keV for the energy of Tc-99m, which was equal to 11% of the photopeak energy, and 9.3 keV for the energy of Tl-201, which was equal to 12% of the photopeak energy. Figure 2 shows an example of the energy spectra of a planar image [case 2].

In the simulation, we used a main window [W_{m1}: 127–158 keV] and a subwindow [W_{l1}: 123–126 keV] for Tc-99m (cases 1–4). For Tl-201, we used a main window [W_{m2}: 65–79 keV] and two subwindows [W_{l2}: 61–64 keV and W_{r2}: 80–83 keV] in case 2 and case 4. Also used a main window [W_{m2}: 63–81 keV] and two subwindows [W_{l2}: 59–62 keV and W_{r2}: 82–85 keV] in case 1 and case 3. These window widths and locations were carefully

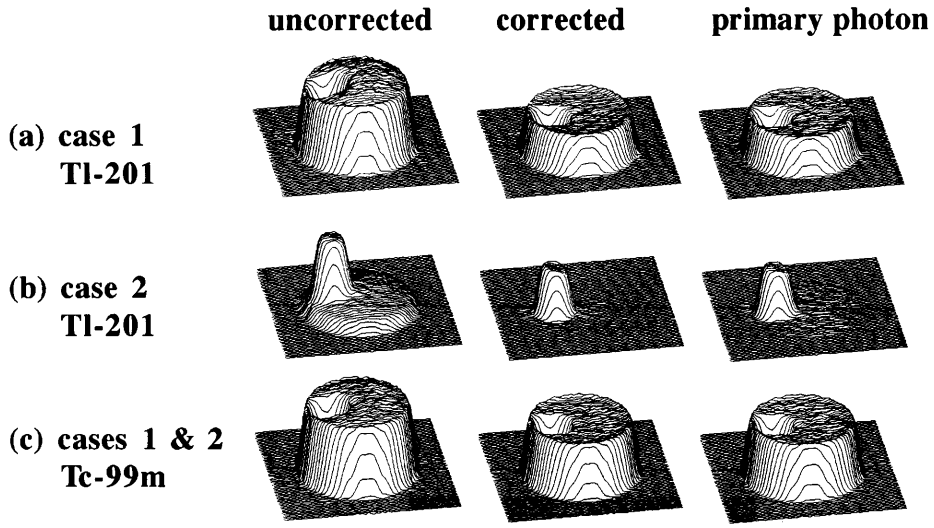

Fig. 3 Reconstructed images in case 1 and case 2. Form left to right, uncorrected images, corrected images, and primary photon images. (a) images of Tl-201 activity (case 1: Tl-201 cold spot with Tc cold spot). (b) images of Tl-201 activity (case 2: Tl-201 hot spot with Tc cold spot). (c) images of Tc-99m activity (cases 1 and 2).

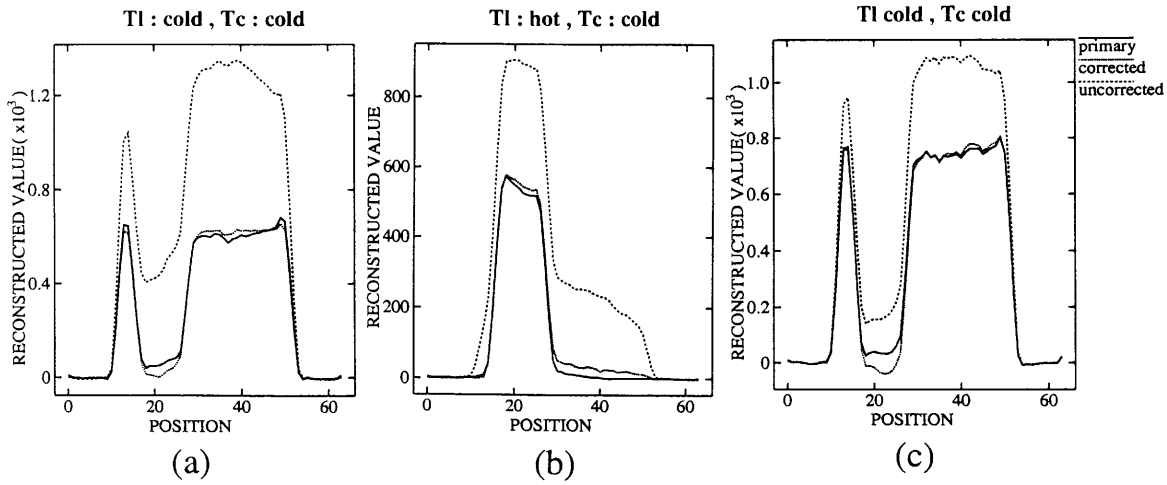

Fig. 4 Profiles of the images in Figure 3. (a) profiles of the images of Tl-201 activity (case 1), (b) profiles of the images of Tl-201 activity (case 2), (c) profiles of the images of Tc-99m activity (cases 1 and 2).

selected to minimize the root mean square difference between corrected images and primary photon images.

The validity of the TEW method was confirmed with images reconstructed from projection data calculated from the spectrum at each position. The projection data were acquired with continuous rotational motion composed of 90 angular samples framed into 4 degrees intervals. The linear sampling interval was 0.5 cm and the projection was composed of 64 bins. Images were reconstructed into a 64 × 64 matrix by a filtered-backprojection method with a Shepp & Logan filter. Attenuation was corrected by a modified version[16] of Chang's method,[17] in which a value of 0.153 [1/cm] for Tc-99m and that of 0.174 [1/cm] for Tl-201 were used as linear attenuation coefficients. We evaluated the images after three iterations of the attenuation correction.

The corrected images were analyzed with the following value:

$$\text{contrast}\ (\%) = \frac{\text{ROIa} - |\text{ROIb}|}{\text{ROIa}} \times 100 \qquad (3)$$

where ROIa and ROIb were the mean values in ROI-a and ROI-b, respectively. The size of the ROI (region of interest) was 6 × 6 pixels. In the hot spot phantom, we positioned the ROI-a and the ROI-b at the center of the inner cylinder and the outer one, respectively. In the case of the cold spot phantom, we located the ROI-a and the ROI-b at the center of the outer cylinder and the inner one, respectively.

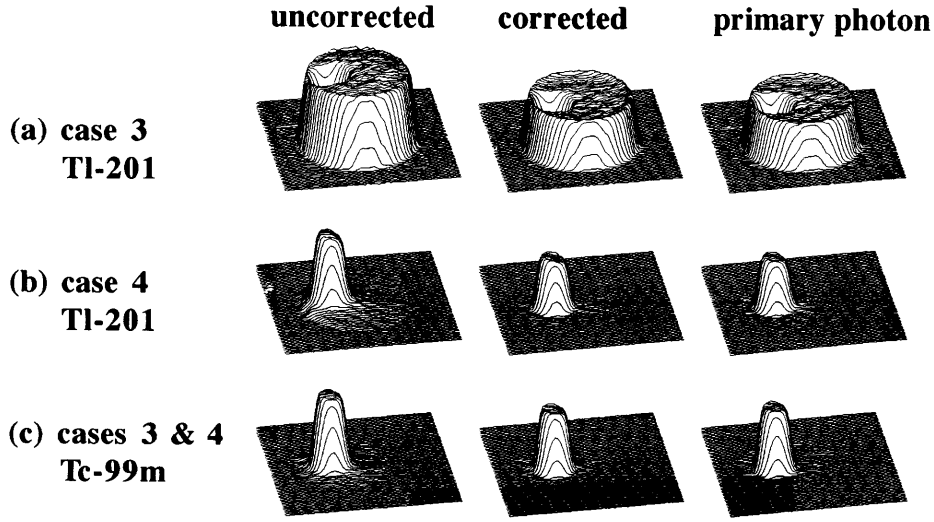

Fig. 5 Reconstructed images in case 3 and case 4. Form left to right, uncorrected images, corrected images, primary photon images. (a) images of Tl-201 activity (case 3: Tl-201 cold spot with Tc hot spot). (b) images of Tl-201 activity (case 4: Tl-201 hot spot with Tc hot spot). (c) images of Tc-99m activity (cases 3 and 4).

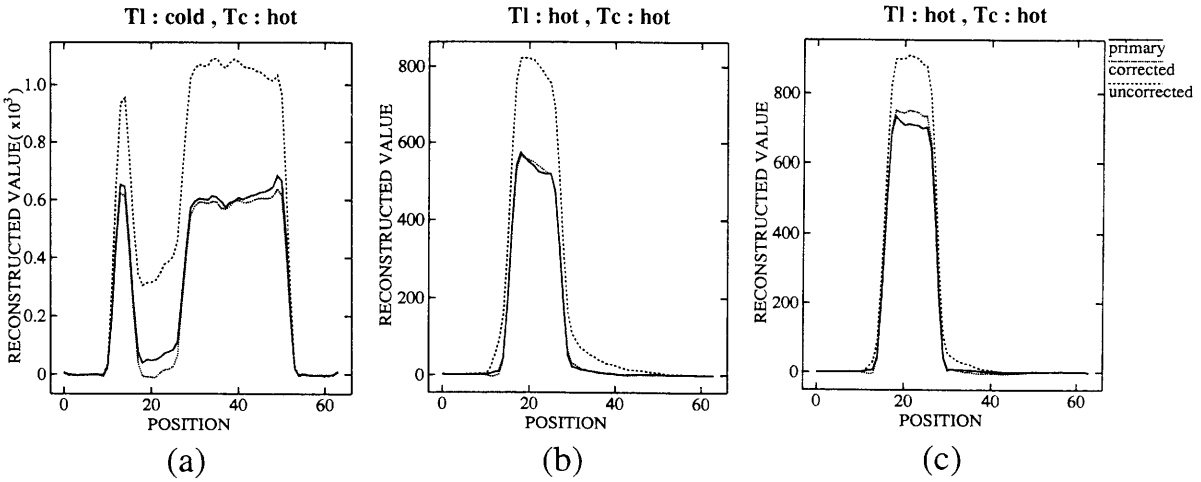

Fig. 6 Profiles of the images in Figure 5. (a) profiles of the images of Tl-201 activity (case 3), (b) profiles of the images of Tl-201 activity (case 4), (c) profiles of the images of Tc-99m activity (cases 3 and 4).

RESULTS

Figure 3 shows the results of simulation [case 1 and case 2]. From left to right, uncorrected images, corrected images, and primary photon images are shown. Figure 3 (a) shows images of Tl-201 activity in case 1, (b) shows those of Tl-201 activity in case 2, and (c) shows those of Tc-99m activity in case 1 and case 2. For both radionuclides, projection data of primary photon images were acquired with a 24% window, and those of uncorrected images were acquired with a 20% window. Figure 4 shows the profiles of the images in Figure 3. The position of the profiles is the center line through the center of the small cylinder. From left to right, (a) Tl-201 distribution (case 1), (b) Tl-201 distribution (case 2) and (c) Tc-99m distribution (case 1 and case 2) are shown. In these cases, there are many scattered photons due to the activity distribution of Tc-99m, but the TEW method yields accurate distribution of Tl-201 for both cold and hot spot phantoms. Figure 5 shows the results of simulation [case 3 and case 4]. In the figure, (a) images of Tl-201 activity in case 3, (b) those of Tl-201 activity in case 4, and (c) those of Tc-99m activity in cases 3 and 4 are shown. Figure 6 shows the profiles of the images in Figure 5. From these results, the corrected images obtained with the TEW method showed good agreement with the ideal images reconstructed from the projection data of primary photons.

Quantitative analysis was done by using a contrast value defined in Eq.(3). The results are shown in Table 1. In the results, image contrast was greatly improved in the

Table 1 Improvement of contrast ratio (%)

	Radionuclide distribution		Contrast (%)†	
	Tl-201	Tc-99m	Tl-201	Tc-99m
case 1	cold	cold	64.5/97.1	85.1/96.1
case 2	cold	hot	67.3/99.5	99.4/99.6
case 3	hot	cold	75.7/96.1	85.1/96.1
case 4	hot	hot	97.5/99.9	99.4/99.6

†(before correction/after correction)

corrected images.

DISCUSSION AND CONCLUSION

In accurately estimating the count of primary photons, an energy spectrum measured with narrow energy windows for each pixel is required. In most clinical cases, however, it is impossible to measure the energy spectrum accurately, and therefore it is hard to estimate the counts of the primary photons accurately from the noisy data. On the other hand, the TEW method does not require an energy spectrum accurately measured by several narrow windows; so the method is less affected by the statistical noise. In case the measured count is not enough, we can enlarge the width of the subwindows and decrease the statistical noise.

Figures 3–6 show that the accuracy of the corrected images of Tl-201 activity does not depend on the distribution of the radionuclide which has high-energy photopeaks. Moreover, Table 1 shows that the corrected images obtained by the TEW method yield a high contrast ratio independent of the distribution of radionuclides having a photopeak of higher energy. These results show that the TEW method is effective in the case of a multiradionuclide SPECT study. In the simulation we assumed that Tl-201 had a single photopeak and the mean energy was calculated from weighted sum of emission probabilities and their energies in several x-rays, but in practice, Tl-201 has a higher energy photopeak than Tc-99m. In this case, we can avoid contamination by Compton photons, which originate in the higher energy gamma ray and enter the Tc-99m photopeak window, by making the subwindow W_{r1}.

In conclusion, the validity of the TEW method in the elimination of the counts of the scattered photons in a multiradionuclide SPECT study was shown by simulation. The results showed the capacity of quantitative SPECT imaging by means of the TEW method and appropriate attenuation correction. Since the method is resistant to statistical noise and yields good estimation of the count of scattered photons, TEW is a practical method to use a SPECT study with multiple radionuclides. In addition, from these results, we can expect that the TEW method will be useful in studies with a single radionuclide having multiple photopeaks such as Ga-67.

REFERENCES

1. Ogawa K, Harata Y, Ichihara T, Kubo A, Hashimoto S. Estimation of scatter component in SPECT planar image using a Monte Carlo method. *Jpn J Nucl Med* 27: 467–475, 1990.
2. Floyd CE, Jaszczak RJ, Harris CC, Coleman RE. Energy and spatial distribution of multiple order Compton scatter in SPECT: a Monte Carlo simulation. *Phys Med Biol* 29: 1217–1230, 1984.
3. Floyd CE, Jaszczak RJ, Coleman RE. Inverse Monte Carlo: A Unified Reconstruction Algorithm for SPECT. *IEEE Trans Nucl Sci* 32: 779–785, 1985.
4. Axelsson B, Msaki B, Israelsson A. Subtraction of Compton-scattered photons in single-photon emission computerized tomography. *J Nucl Med* 25: 490–494, 1984.
5. Jaszczak RJ, Greer KL, Floyd CE, Harris CC, Coleman RE. Improved SPECT quantification using compensation for scattered photons. *J Nucl Med* 25: 893–900, 1984.
6. Koral KF, Swailem FM, Buchbinder S, Clinthone NH, Rogers WL, Tsui BMW. SPECT dual-energy-window Compton Correction: Scatter Multiplier Required for Quantification. *J Nucl Med* 31: 90–98, 1990.
7. Hamill JJ, DeVito RP. Scatter reduction with energy-weighted acquisition. *IEEE Trans Nucl Sci* 36: 1334–1339, 1989.
8. Koral KF, Wang X, Rogers WL, Clinthorne NH, Wang X. SPECT Compton-scattering correction by analysis of energy spectra. *J Nucl Med* 29: 195–202, 1988.
9. Gagnon D, Todd-Pokropek AE, Arsenault A, Dupras G. Introduction to holospectral imaging in nuclear medicine for scatter subtraction. *IEEE Trans Med Imag* 8: 245–250, 1989.
10. Floyd CE, Jaszczak RJ, Coleman RE. Scatter detection in SPECT imaging: dependence on source depth, energy, and energy window. *Phys Med Biol* 33: 1075–1081, 1988.
11. Koral KF, Clinthorne NH, Rogers WL. Improving emission-computed-tomography quantification by Compton-scatter rejection through offset window. *Nucl Inst and Methods in Phys Res* A242: 610–614, 1986.
12. King MA, Hademenos GJ, Glick SJ. A dual photopeak window method for scatter correction. *J Nucl Med* 33: 605–612, 1992.
13. Ogawa K, Harata Y, Ichihara T, Kubo A, Hashimoto S. A Practical method for position-dependent Compton-scatter correction in single photon emission CT. *IEEE Trans Med Imag* 10: 408–412, 1991.
14. Ichihara T, Ogawa K, Motomura N, Kubo A, Hashimoto S. Compton scatter correction using triple-energy window method for single- and dual-isotope SPECT. *J Nucl Med* 34: 2216–2221, 1993
15. Raeside DE. Monte Carlo principles and applications. *Phys Med Biol* 21: 181–197, 1976.
16. Ogawa K, Takagi Y, Kubo A, Hashimoto S, Sanmiya T, Okano Y, et al. An attenuation correction method of single photon emission computed tomography using gamma ray transmission CT. *KAKU IGAKU (Jpn J Nucl Med)* 22: 477–490, 1985.
17. Chang LT. A method for attenuation correction in radionuclide computed tomography. *IEEE Trans Nucl Sci* 25: 638–642, 1978.